ACCSCIENCE PUBLISHING

Materials Science in Additive Manufacturing

ORIGINAL RESEARCH ARTICLE

On the surface integrity resulting from laser powder bed fusion of Ti6Al4V: Improvements by cavitation abrasive surface finishing

Rohin Petram[1†], Conall Wisdom[1†], Alex Montelione[1†], Cole Nouwens[2], Angelina Martinez[1], Marquiz Silvestre[1], Dan Sanders[2,3*], Mamidala Ramulu[2], and Dwayne Arola[1,2*]

[1]Department of Materials Science and Engineering, University of Washington, Seattle, Washington, United States of America

[2]Department of Mechanical Engineering, University of Washington, Seattle, Washington, United States of America

[3]Sugino Machine Ltd., Toyama, Japan

Abstract

As the manufacturing readiness level of laser powder bed fusion (L-PBF) advances, post-processing has become increasingly important for achieving net-shape components and to enhance surface texture and integrity. Apart from surface roughness, one concern is the unique morphology of printed surfaces with vertical, upskin, and downskin inclinations. In this study, we characterized the surface texture and integrity of L-PBF Ti6Al4V with respect to build orientation. In the as-built condition, the downskin surfaces possessed the highest roughness, the largest effective surface stress concentration ($\overline{K_t}$), and the greatest presence of partially melted powder particles fused to the surface. Cavitation abrasive surface finishing (CASF) was adopted to improve surface quality, with consideration of the build orientation. The results indicated that CASF reduced roughness, lowered K_t posed by the surface texture, and introduced compressive residual stress regardless of the build orientation. Downskin surfaces were the most challenging to treat; they exhibited substantially greater $\overline{K_t}$ than the other orientations after treatment (>2×) and lower compressive residual stress (50%). More extensive powder coverage of the downskin surfaces appears to shield the underlying substrate from abrasive attack and direct implosion of cavitation bubbles, which are central to the CASF treatment mechanism. The importance of orientation to the effectiveness of CASF treatment is discussed, as well as strategies to overcome this challenge. Overall, downskin surfaces require greater surface treatment intensity or duration to obtain the same degree of improvement.

Keywords: Additive manufacturing; Laser powder bed fusion; Post-processing; Residual stress; Roughness; Stress concentration; Surface treatment; Titanium

1. Introduction

Laser powder bed fusion (L-PBF) is a method of additive manufacturing (AM) that involves sequential deposition and melting of metal powder in a layer-by-layer process

†These authors contributed equally to this work

***Corresponding authors:**
Dwayne Arola
(darola@uw.edu)
Dan Sanders
(dsanders@suginocorp.com)

Citation: Petram R, Wisdom C, Montelione A, *et al*. On the surface integrity resulting from laser powder bed fusion of Ti6Al4V: Improvements by cavitation abrasive surface finishing. *Mater Sci Add Manuf*. 2026;5(1):025280062. doi: 10.36922/MSAM025280062

Received: July 12, 2025

Revised: August 15, 2025

Accepted: August 15, 2025

Published online: October 14, 2025

to produce components of desired geometry. Notably, there are several advantages of L-PBF over traditional manufacturing techniques (*e.g.*, forging and machining), including comparatively low material waste, nearly unlimited geometric complexity, and the capability for producing customized components simultaneously in a single build.[1-4] While the geometric complexity achievable with L-PBF enables the manufacture of components unattainable by traditional methods,[5] it also introduces challenges. Specifically, increasing geometric complexity limits the available methods for post-processing of L-PBF components and their effectiveness.[6]

Fatigue is an important design consideration for many components produced by L-PBF, especially for those of titanium alloys.[7-12] It is widely recognized that the fatigue life of metal components is highly dependent on the surface texture and integrity resulting from the methods of processing.[13,14] Rough surfaces create stress concentrations that can reduce strength, depending on the level of ductility, as well as accelerate fatigue crack initiation and fatigue failure.[15-17] As such, surface quality and the corresponding surface topography, associated with the lay and profile valley distribution, are important to the overall fatigue performance of engineering components.[18-21] Components that are produced by powder bed fusion (PBF), including electron beam and laser, are recognized for their high surface roughness in the as-built condition, making surface integrity a major concern.[22-24] To reduce the detrimental effects of these surface qualities, L-PBF parts often require post-processing to improve their surface integrity.[25-27]

A unique aspect of metal components produced by PBF is that the surface texture is dependent on the geometric complexity and orientation of the part surface relative to the build plane.[5,6,28-31] To address metrology challenges, Cabanettes *et al.*[5] performed a detailed analysis of surfaces developed by L-PBF. They evaluated the utility of various methods for characterizing surface texture and roughness parameters for describing the quality and discriminating the effects of build/surface orientation. Equally relevant, the wide range of surface orientations in the build and their corresponding characteristics can affect the effectiveness of post-processing techniques employed to improve surface quality.[6] There are three primary surface orientations to consider. Component surfaces that are orthogonal to the build plane are regarded as vertical surfaces and do not incline relative to the incident laser. In contrast, when the exposed surface has an inclination and is facing upward toward the incident laser, it is referred to as an upskin surface. Upskin surfaces are supported by previously solidified metal layers underneath, and they typically exhibit less partially melted powder adhered to the surface.[22,32] In contrast, downskin surfaces face toward the build plate and are oriented toward unmelted powder without a previously solidified metal layer. This surface inclination typically results in higher levels of powder melted or sintered to the exterior surface.[22,32,33] Relevant to this specific surface topography is the "staircase" or stair-stepping effect.[34,35] However, partially melted powder accumulated on the surface can mask the staircase quality. Surfaces that are printed vertically do not exhibit the same staircase geometry and typically display intermediate powder concentrations. Therefore, components that are manufactured by L-PBF can have substantially different surface morphology in different areas, and assessments of new post-processing treatments should consider this variation in surface characteristics.

At present, chemical milling serves as the industry standard for reducing the roughness of L-PBF parts and is widely regarded as an effective method for improving surface finish.[36-38] However, due to the hazardous and toxic chemicals involved, there are workforce and environmental concerns with chemical milling.[39] In addition, if improving fatigue resistance is the objective of surface treatment, there are three aspects of consideration: surface roughness, effective stress concentration, and the residual stress.[40] While chemical milling is effective at removing material, it is not capable of introducing compressive residual stresses, a key component to improving the fatigue resistance of metallic parts. Shot peening can introduce residual stress, but requires line of sight, which is less compatible with complex AM parts that are designed with passages or internal cavities.[41,42] Several other peening techniques do not use solid shot particles. Waterjet peening (WJP)[43] and abrasive WJP,[44-46] a derivative of WJP, are potential surface treatment processes. Alternatively, cavitation peening uses a cavitating waterjet to peen the surface through the implosion of vapor bubbles.[47] While cavitation bubbles are often introduced by waterjet processes, they can also be induced using laser pulses and ultrasonic waves. However, limited information is available concerning the degree of smoothing and resulting residual stress applied to metal additive components using these methods.[47,48]

Cavitation abrasive surface finishing (CASF) is a variant of cavitation peening, whereby a cavitating waterjet is used to peen the surface of the targeted component that is submerged within an abrasive slurry tank. The implosion of the cavitation bubbles energizes the abrasive particles in the slurry, facilitating material removal and reducing surface roughness. Simultaneously, when cavitation bubbles implode upon contacting the part surface, they generate shock waves that induce localized plastic deformation and introduce compressive residual

stresses in the near-surface layers.[49-51] The nature of the CASF method of impingement has several advantages over its more well-known contemporaries. First, the slurry of water and abrasives is environmentally inert and does not pose the same risk as the acids used in chemical milling. In addition, compared to other treatments that are capable of reducing surface roughness or introducing compressive residual stress, CASF is capable of improving both of these qualities simultaneously.[36,37,52] However, it is unclear how the process varies when applied to surfaces with different textures arising from unique build orientations, and this aspect of treatment effectiveness has received limited attention.[52]

In this investigation, Ti6Al4V samples were printed by L-PBF with either vertical, upskin, or downskin orientations. The objective of this study was to evaluate the effectiveness of CASF surface treatment in improving the surface integrity of L-PBF Ti6Al4V parts with respect to the as-built condition. The improvements were characterized by changes in residual stress, surface texture, and surface stress concentration over several different printing orientations. The printed surfaces were characterized in terms of the surface roughness, effective stress concentration posed by the dominant valleys, and both the surface and subsurface residual stress. In addition, selected samples underwent CASF treatment at oblique angles of impingement to evaluate the effectiveness of non-orthogonal treatment. The unique capabilities of the CASF process and limitations are highlighted with respect to other post-processing methods.

2. Methods

2.1. Sample preparation

In this study, samples were prepared using Ti6Al4V powder via L-PBF with an EOS M290 printer (Electro Optical Systems, Germany). The Ti6Al4V powder was used in prior production builds and thus was in the "reused" condition without provenance. Additional details regarding the vendor, number of prior builds, or hours of exposure were not available. Nevertheless, the powder conformed to the requirements outlined in ASTM F2924,[53] which establishes the composition limits of potential contaminants. These details are not highly relevant to assessing the effects of the CASF process on surface texture and integrity.

The printed samples consisted of rectangular plates with a width and length of 25 and 50 mm, respectively, and with thicknesses of 2, 4, and 6 mm. Half of the plates were printed with vertical orientation, aligned parallel with the XZ-plane (as defined by ASTM 52921).[54] The other half was printed with the same orientation but with an offset angle of 45° with respect to the XZ plane (Figure 1A). Plates printed with 45° offset provided an upskin and downskin surface with identical orientation as the vertical surfaces. Printing was conducted in accordance with manufacturer-recommended settings, which were the default settings for Ti6Al4V.

2.2. Post-processing

After printing, the builds were heat-treated in an argon environment at 745°C for 2 h. The plates were then removed from the build plate using a band saw, and the stabilizing brackets and other unnecessary support structures were removed. The plates were then subjected to CASF treatment at Sugino Machine Ltd. (Toyama, Japan), using a newly developed automated system with computer numerical control. The plates were clamped along the edges, and a CASF jet was passed over the samples with a standoff distance from nozzle to plate surface of 50 mm. The CASF jet traversed along the major axis of the plate, which was perpendicular to the lay of the surface introduced by the layerwise progression of the build. Each pass was 4 mm apart, and the initial and final passes were outside the bounds of the plate to ensure complete treatment (Figure 1B). The slurry tank consisted of alumina abrasives with #200 mesh and approximately 30% abrasive concentration by weight. Several treatments were conducted, which spanned a jet traverse rate of 60–120 mm/min. These parameters were selected in partnership with Sugino Machine Ltd., based on an internal preliminary investigation that distinguished the most appropriate range of treatment conditions for this scoping study.

2.3. Surface texture

After the CASF treatments were conducted, the surfaces were evaluated using a commercial contact profilometer (Mahr MarSurf GD 25, Mahr, United States of America [USA]) with an MFW II Tip attachment having a 90° angle and 2 µm radius of curvature. Three-line scans were conducted for each specimen; all scans were performed along the major axis of the plate in the build direction, which is perpendicular to the principal lay to capture the surface height variation of the additive layers. For each profile, the average roughness (R_a), 10-point roughness (R_z), and peak to valley height (R_y) were calculated according to the ISO 4288 standard.[55] As defined by this standard, for a measured R_a of ≤10 µm, a cutoff length of 2.5 mm and traverse length of 15 mm were used. Some of the roughness scans produced an R_a above 10 µm. According to the ISO 4288 standard, a larger cutoff length and traverse length should be used to calculate roughness for these samples. However, the measurement stroke of the profilometer was only 25 mm long, negating the potential for the 8 and 48 mm cutoff and traverse lengths. As such, the longer scan

was not possible, and all roughness measurements used the 2.5 mm cutoff length.

2.4. Stress concentration factor

The profile data exported from the profilometer was used to select the most prominent valleys of each surface. Then, a graphical radius gauge was used to estimate the radius of curvature according to previously reported methods.[15,16] The six deepest valleys of each roughness scan were selected to estimate the degree of stress concentration. The root radius (ρ) of each valley was estimated graphically (Figure 2). The effective stress concentration factor ($\overline{K_t}$) was then calculated using the following equation:

$$\overline{K_t} = 1 + n\left(\frac{R_a}{\overline{\rho}}\right)\left(\frac{R_y}{R_z}\right) \quad \text{(I}$$

where the R_a, R_z, and R_y values refer to the arithmetic average roughness, 10-point roughness, and peak-to-valley roughness measurements, respectively. The value ($\overline{\rho}$) refers to the average profile valley radius estimated from the six dominant valleys assessed over the profile traverse length. According to this approach, the estimated ($\overline{K_t}$) for each surface represents the upper bound of stress concentration, which is represented by the family of notches present in the topography. Analysis of variance (ANOVA) was conducted to evaluate differences in the measured $\overline{K_t}$ values, with significance defined by a $p<0.05$.

2.5. Residual stress measurements

Residual stress in the Ti6Al4V samples was measured using the $\sin^2(\psi)$ measurement method.[56] X-ray diffraction was performed using a Bruker D8 Discover diffractometer

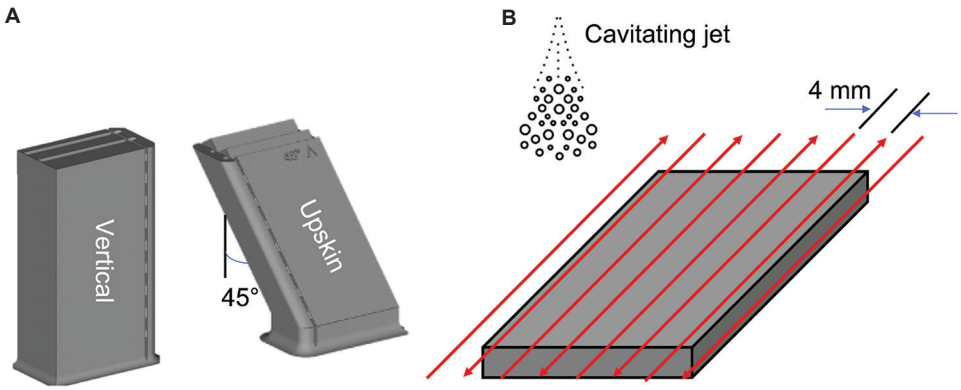

Figure 1. Samples and treatment. (A) The samples were built in clusters of rectangular plates with 2, 4, and 6 mm thickness and with either a vertical or 45° orientation. The 45° orientation provided surfaces with an upskin or downskin inclination. (B) The plate surfaces were treated by cavitation abrasive surface finishing with a raster pattern consisting of a 4 mm path center offset

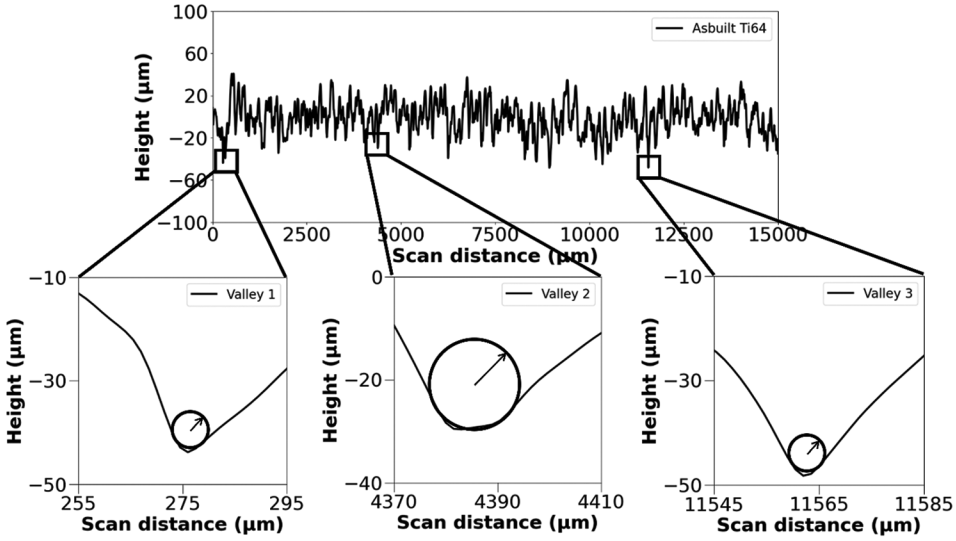

Figure 2. Representative surface profile from an as-built surface with vertical build orientation and measurement of selected profile valley root radii (ρ)

(Bruker, USA) equipped with a copper target (Cu Kα) operating at 50 kV and 1000 μA. A 0.5 mm collimator was used to focus the beam, and measurements from the diffracted [312] plane at 2θ = 110° were recorded using a Pilatus 100K large-area 2D detector. Each sample was analyzed at nine distinct orientations, combining Φ angles of 0°, 45°, and 90° with ψ angles of 0°, 22.5°, and 45°. The detector captured a 2θ range of 107°–113° over a 4-min scan for each orientation.[57] Residual stress values were determined from the diffraction peak positions using Bruker's Diffrac.Leptos7 software (Bruker, USA).

To measure residual stress as a function of depth beneath the treated surface, a sequential etching technique was used to remove material from the surface a few microns at a time without changing the underlying residual stress profile. Specifically, Kroll's reagent (etchant #192 of ASTM E407-7)[58] was applied for 3 min and then rinsed off with DI water. After each etching session, a micrometer was used to measure the remaining sample thickness, which was then used to calculate the thickness of material removed by etching. This process was repeated multiple times to achieve measurements as a function of depth, continuing until the depth at which no residual stress was detectable. To enhance the statistical power of the measurements, the treated surface was divided into four quadrants, and the residual stress was measured in each. These quadrants were then outlined with a thin layer of nail polish. The nail polish acted as a masking agent to protect the metal that it covered.

2.6. Microscopy

Scanning electron microscopy (SEM) was performed to observe the detailed surface morphology and validate the roughness measurements. The SEM analysis was performed using an Apreo-S SEM (ThermoFisher Scientific, USA) at voltage and current values of 25 kV and 3.2 nA, respectively.

To characterize changes in the surface texture resulting from CASF, the treated specimens were sectioned to expose the layered structure of the AM material for optical imaging. The specimens were mounted in black glass-filled epoxy (Allied 150-10105, Allied High Tech Products, Inc., USA) in cylindrical molds. The exposed surfaces were then polished using silicon carbide abrasive mesh pads from #240 to #800 mesh to level the surface (Allied 50 series, Allied High Tech Products, Inc., USA). Subsequently, abrasive polishing was performed using a 9 μm DiaLube diamond suspension on a Struers MD-Dac pad (Struers, USA), followed by a chemical polishing on a Struers MD-Chem pad with a solution of 10 mL 0.05 μm colloidal silica, 0.5 mL 5% ammonium hydroxide, and a few drops of 40% hydrogen peroxide. Micrographs were taken from the polished cross-section using an Olympus BX51M optical microscope (Olympus, USA) at between 5× and 50× magnifications.

3. Results

3.1. Surface morphology and texture

Representative SEM images of the sample surfaces in the as-built condition are displayed in Figure 3A-C for the vertical, upskin, and downskin inclinations, respectively. As evident from these images, numerous partially melted particles adhered to the substrate, and the density of coverage depends on the build orientation. The layer orientation is visible in the horizontal plane for both the vertical and upskin surfaces, whereas it is obscured on the downskin surface due to the higher density of adhered particles. Based on image analysis, estimates for the particle count were roughly 250, 40, and 540 particles/mm^2, respectively; these differences are statistically significant ($p \leq 0.05$).

The average surface roughness for the surfaces with vertical, upskin, and downskin inclinations is presented in Figure 4 as a function of treatment feed rate. The shaded background represents the range of roughness in the as-built condition, whereas the R_a values after CASF treatment are presented for each surface orientation as the mean ± standard deviation from three profiles. The direction of measurement is parallel to the build direction (z-axis), which is perpendicular to the layer orientation noted in Figure 2. As evident from Figure 4, CASF treatment reduced roughness for all three printing orientations across all feed rates. The largest reduction in R_a occurred on surfaces with a vertical orientation. Although the vertical and downskin surfaces displayed similar maximum reduction in roughness (approximately 50%), the downskin orientation had the highest roughness after CASF treatment. In addition, the downskin surfaces exhibited the highest sensitivity to the treatment feed rate, with a decrease of approximately 10 μm at the lowest feed rate. In contrast, the upskin surfaces exhibited a reduction in Ra of approximately 30% following CASF treatment, but the feed rate had no significant influence on the outcome.

3.2. Stress concentration

In addition to evaluating surface roughness, the radius of curvature (ρ) of the prominent valleys was measured for the three surface orientations in the as-built condition and after CASF. The effective valley root radii ($\bar{\rho}$) representing the average values are shown in Figure 5A as a function of the treatment feed rate. In the as-built condition, the valley radii ranged from 3 to 15 μm, independent of the

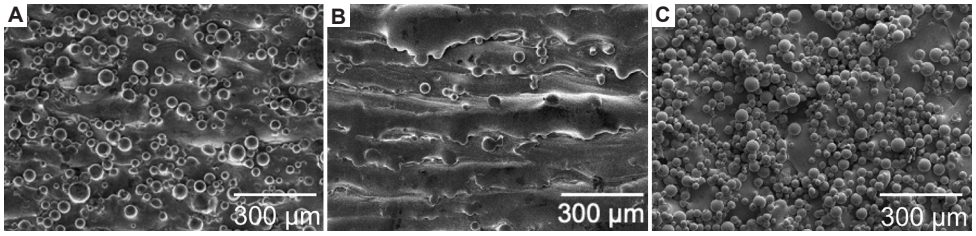

Figure 3. Scanning electron microscope images of the (A) vertical, (B) upskin, and (C) downskin surfaces in the as-built condition. The build direction is from bottom to top. The upskin and downskin surfaces resulted from printing a plate with a 45° inclination. Scale bars: 300 µm

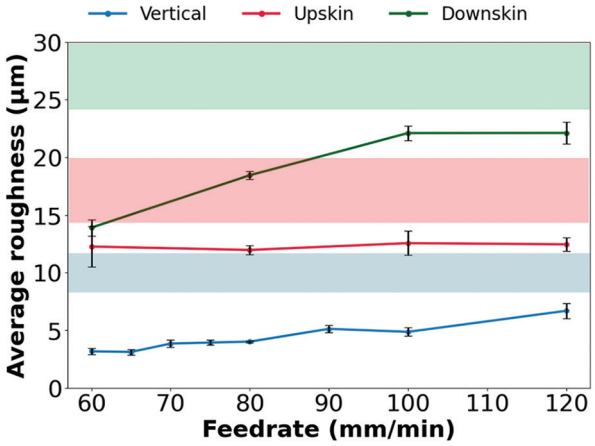

Figure 4. Comparison of the average surface roughness for the three surface orientations (vertical, upskin, and downskin) as a function of feed rate. The colored lines indicate the average roughness for each printing orientation (n = 5), and the lighter colored bars in the background represent the range of roughness in the as-built condition for the three surface orientations

orientation. Surprisingly, CASF treatment increased the $\overline{\rho}$, but only for the vertical orientation and at the lowest feed rate. In comparison, there are essentially negligible increases in the profile valley radii of the upskin and downskin surfaces after CASF treatment.

The effective stress concentration factor ($\overline{K_t}$) of the surfaces for the as-built condition and after CASF treatment is presented in Figure 5B. The importance of surface orientation is further apparent in the changes in $\overline{K_t}$ before and after treatment. Most notable is the reduction in stress concentration for the vertical orientation, approaching a stress concentration of 1 at the lowest feed rate. The reduction in $\overline{K_t}$ for the downskin surfaces is significant, ranging between 50% and 75% reduction over the feed rate range. The upskin surfaces exhibited the smallest reduction in $\overline{K_t}$ overall, with only a slight reduction at higher feed rates. Due to the absence of changes in $\overline{\rho}$ for the upskin and downskin conditions (Figure 5A), the reduction in $\overline{K_t}$ for these surfaces appears to be limited to the reduction in surface roughness. ANOVA results indicated that changes in $\overline{K_t}$ values with feed rate were significant ($p \leq 0.05$) for all orientations, except for the upskin orientation.

3.3. CASF treatment orientation

Several complementary CASF treatments were conducted to assess the influence of jet incident angle on the improvement of the surface quality. Performed as a preliminary effort, these experiments were conducted using the vertically printed samples, which were fixtured at a 45° angle with respect to the incident jet. These treatments were compared with the results of those conducted with a normal impingement angle (90°). Results for the R_a and $\overline{K_t}$ responses are displayed in Figures 6 and 7, respectively. As evident in Figure 6, treatment with non-orthogonal orientation resulted in lower reduction in roughness and higher post-treated roughness than the 90° orientation. Although the differences between the R_a for the 90° and 45° treatment orientations were significant over the majority of feed rates ($p \leq 0.05$), the difference was limited to approximately only 1 µm for all feed rates. The influence of treatment orientation on $\overline{\rho}$ and $\overline{K_t}$, as featured in Figure 7A and B, follows similar trends to the surface roughness. Although a reduction in treatment angle slightly diminished effectiveness—particularly at lower feed rates—the angled treatments still produced a substantial decrease in $\overline{K_t}$. As evident from Figure 6, this reduction in $\overline{K_t}$ is primarily attributed to the decrease in surface roughness rather than changes in $\overline{\rho}$.

3.4. Residual stress

Figure 8 features the surface residual stress distribution in samples printed with the vertical, upskin, and downskin orientations at different feed rates. All conditions resulted in compressive residual stress. While no clear dependence on feed rate was observed, a significant difference ($p \leq 0.05$) was found between the build orientations. Specifically, the upskin orientation had the highest residual stress, followed

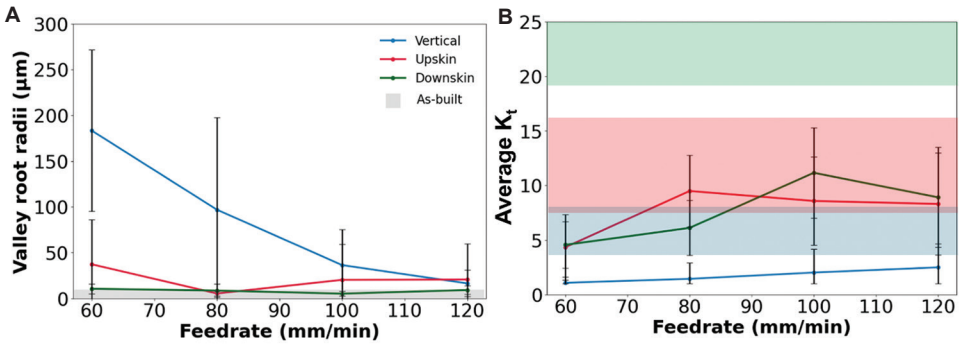

Figure 5. Comparison of surface characteristics of the three orientations (vertical, upskin, and downskin) after treatment and across different feed rates. (A) Effective valley root radii ($\bar{\rho}$) (n = 5). The gray bar represents the range in valley radii in the as-built condition for all three surface orientations. (B) Effective stress concentration factor ($\overline{K_t}$) (n = 5). The colored bars represent the $\overline{K_t}$ range for the as-built condition

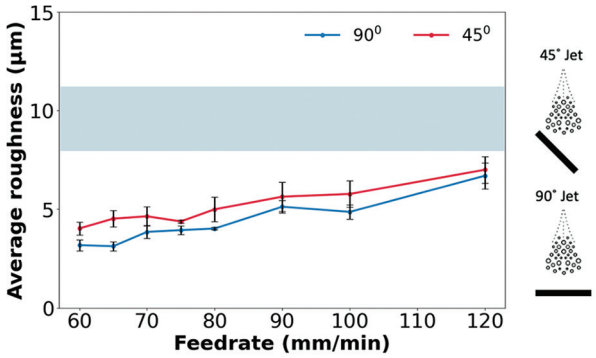

Figure 6. Comparison of average roughness for the vertically printed plates as a function of feed rate and the CASF treatment angle (n = 5). The light blue bar represents the range of as-built roughness before treatment
Abbreviation: CASF: Cavitation abrasive surface finishing

by the vertical and downskin orientations. This trend appears to correlate with the extent of powder coverage on the surface (Figure 3), suggesting that the residual stress introduced by CASF depends on the degree of powder coverage, which may inhibit deformation of the underlying substrate.

Figure 9 displays the influence of treatment orientation (45° vs. 90°) on the residual stress for samples printed with a vertical orientation. Akin to the trends in roughness (Figure 6), there was no significant difference in residual stress over the tested feed rates. However, the differences associated with the impingement angle were significant. Independent of feed rate, treated samples with a 45° impingement angle exhibited approximately 50% lower residual stress than treated surfaces with an orthogonal jet arrangement ($p \leq 0.05$).

Figure 10 presents the residual stress distribution within a single vertical orientation sample as a function of depth beneath the surface. The sample was treated with the jet oriented orthogonal to the surface and at a feed rate of 80 mm/min. The subsurface stress was measured at four different positions on the samples. The residual stress was highly consistent across all sites, with surface stress of approximately 400 MPa, in agreement with the distribution displayed in Figure 8. The stress decreased to 80 MPa within 30 µm from the treated surface, and measurements beyond this depth featured no further reduction in residual stress.

4. Discussion

The results revealed that CASF has the potential for improving the overall surface quality of Ti6Al4V components produced by L-PBF, as observed by the reduced surface roughness, a decrease in $\overline{K_t}$, and the introduction of compressive residual stress. However, the effectiveness of the process is influenced by both the printed surface orientation and the jet impingement angle, which warrants further discussion.

For all printing orientations and feed rates, the CASF process resulted in a reduction in R_a (Figure 4). Considering all three build orientations, the highest reduction occurred at the lowest feed rate. Notably, the treatment intensity increases with decreasing feed rate, which reflects the treatment duration per unit area. Moreover, the degree of improvement over the range of feed rate was not consistent among the three orientations. The upskin surfaces exhibited negligible changes at lower feed rates, whereas the downskin surfaces underwent significant improvement when the feed rate was reduced from 120 to 60 mm/min; the vertically printed metal exhibited a trend between these two extremes.

The orientation dependence in roughness improvements can be attributed to the particle coverage evident in Figure 3, which affects two components of smoothing: (i) the removal of partially melted particles through erosion, and (ii) the abrasive wear of the substrate peaks beneath

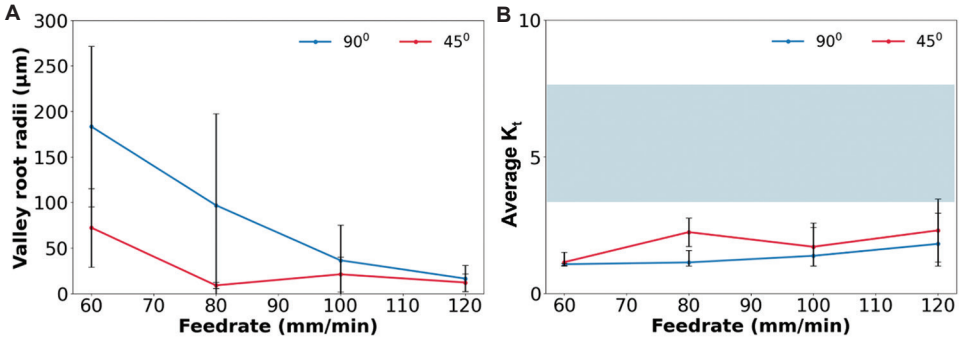

Figure 7. Comparison of surface characteristics of the two treatment orientations at different feed rates: (A) valley root radii and (B) effective stress concentration factor (K_t) ($n = 5$). The light blue shaded area indicates the range of K_t before CASF treatment
Abbreviation: CASF: Cavitation abrasive surface finishing

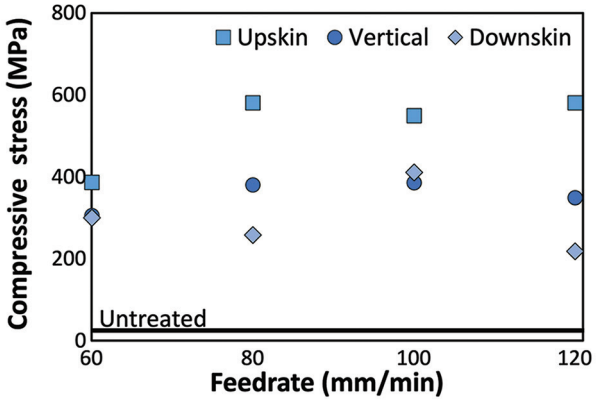

Figure 8. Comparison of compressive residual stress induced by CASF across the range of feed rates for samples with three build orientations: Vertical, upskin, and downskin surfaces
Abbreviation: CASF: Cavitation abrasive surface finishing

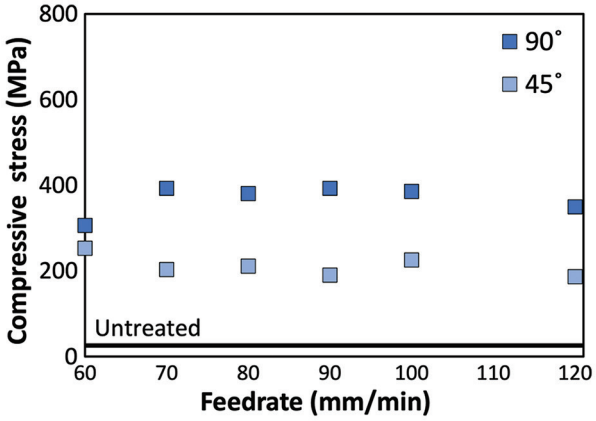

Figure 9. Comparison of residual stress from CASF treatment with jet impingement angles of 45° and 90°
Abbreviation: CASF: Cavitation abrasive surface finishing

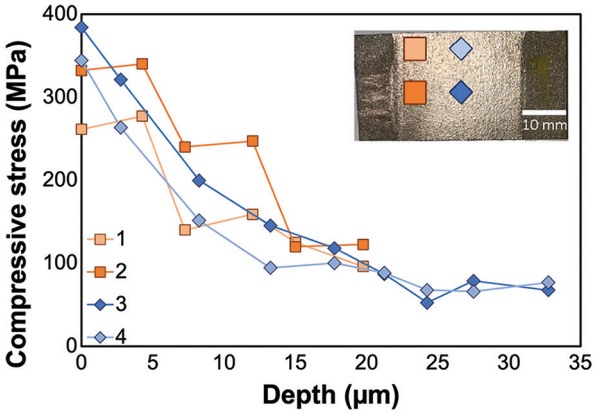

Figure 10. Subsurface residual stress gradient at four different locations. CASF treatment was conducted at a feed rate of 80 mm/min on a 6 mm thick vertically oriented L-PBF sample. Scale bar: 10 mm (inset)
Abbreviations: CASF: Cavitation abrasive surface finishing; LPBF: Laser powder bed fusion

the particle coverage. The more extensive changes in the downskin surface appear to result from the removal of the powder layer, which is most effective at low feed rates. In the case of the upskin surface, nearly all changes are related to the second component, i.e., abrasive wear, whereas the increase in treatment intensity coupled with a reduction in feed rate had a limited effect. Therefore, optimizing the effectiveness of CASF will require special consideration of feed rate as it relates to the metal target properties and build orientation. A slower feed rate should be applied to the downskin regions, whereas a higher speed could be used during the treatment of vertical and upskin surfaces. A full parametric study is warranted to further improve the effects of CASF treatment. Abrasive size, standoff distance, slurry concentration, and raster spacing are all parameters that could be explored and considered in the treatment of primary material candidates.

Although measurable, the difference in roughness reduction of the vertically printed surfaces treated by CASF at 90° and 45° was limited. This indicates that

CASF can significantly improve L-PBF surface quality even when the jet is not directly perpendicular to the surface. Such flexibility is advantageous for treating metal AM components with complex geometries, as well as the commercial viability of CASF as a practical finishing method. Both surface texture and integrity can be enhanced even under oblique treatment angles.

The reduction in R_a of L-PBF components using CASF depends on the as-built condition of the surface metal and the extent of powder coverage. For vertically printed samples, R_a decreased from approximately 10 μm to as low as 4 μm, which is comparable to shot peening (≈ 4 μm)[40,41] and appears superior to laser shock peening (≈ 15 μm).[40,59] It is important to highlight that comparing surface roughness results from different treatments is limited by the variability of AM parts, including the treatment parameters, the starting surface texture, and powder coverage. Figures 4 and 5 suggest that CASF is more effective at lower feed rates, though this may reduce productivity unless other parameters are adjusted. Further development efforts could potentially achieve surface quality comparable to leading industry treatments, including laser polishing and centrifugal finishing.[40]

The primary objective of applying CASF is arguably to improve the fatigue life of L-PBF components. An important aspect of the surface structure that contributes to fatigue crack initiation is the root valley radii (ρ).[60-63] Interestingly, while there was a reduction in $\overline{K_t}$ for all surfaces evaluated, the increase in $\overline{\rho}$ was most substantial for the vertical surfaces and at the lowest feed rates. Meanwhile, the upskin and downskin surfaces exhibited less improvement across the full feed rate range. For downskin surfaces, this is partly due to powder coverage, but it also relates to valley geometry—profile valleys between layers are too deep for the abrasives to fully smooth. In addition, the orientation of layer boundaries on upskin and downskin surfaces makes them more pronounced, providing shielding that limits CASF effectiveness.

The difference in surface structures is important to understanding their treatability. Cross-sectional views of the treated surfaces for the three build orientations are displayed in Figure 11. While most of the surface has undergone smoothing and reduction in surface height variation, some regions have notch-like residual features. These are apparent in the cross-sections of the upskin and downskin surfaces (Figures 11 and 12). The angular offset of the layers, combined with gravity, produced narrow valley openings, much smaller than the abrasive diameter, shielding them from CASF treatment while remaining potential sites for fatigue crack initiation. Although cross-sections are commonly used to study particle attachment, there is limited focus on valley geometry, orientation-related differences, and residual features that threaten durability.[5,34,64] The higher initial roughness of the upskin and downskin surfaces, combined with the aforementioned aspects of valley orientation, hampers the effectiveness of CASF. Residual valleys that are not fully treated remain a concern for these orientations. Designing L-PBF components for effective post-processing could minimize fatigue-critical regions in upskin and downskin areas, but the most impactful approach would be to enhance CASF effectiveness for these more challenging orientations.

Residual stress analysis revealed that CASF feed rate had little effect on surface stress, whereas printed build orientation played a significant role. Specifically, the highest surface residual stress reached up to 600 MPa and was observed in the upskin surfaces. The vertical and downskin surfaces reported surface stresses of 350 and 250 MPa, respectively. Comparison with the as-built surface morphology (Figure 3) indicates an inverse correlation between residual stress and the density of surface powder particles. The interaction of the CASF jet with these powder particles does not generate residual stress. Mechanistically, the cavitation bubbles are shielded from implosion on the underlying substrate until the partially melted particles are removed by erosion. Consequently, surfaces with lower particle density, such as upskin and vertical orientations, experience greater substrate deformation during treatment, resulting in higher residual stress. Optimizing CASF parameters to first remove particle coverage and then maximize residual stress, or combining CASF with complementary surface treatments, could further enhance this effect.

In addition to surface morphology, the impingement angle was identified as a key factor contributing to residual stress (Figure 9). Compressive residual stresses induced by CASF are greatest when the treatment is orthogonal to the surface. While smoothing during CASF is not largely dependent on the impingement angle (Figures 6 and 7), treating at an oblique angle can reduce surface residual stress by nearly 50% compared to a 90° angle. These results suggest that to maximize residual stress, the surfaces should be oriented orthogonal to the incident jet, which also results in the maximum degree of smoothing and reduction of the $\overline{K_t}$. However, if surface texture is the primary concern and residual stress is less critical, oblique treatment is acceptable.

In addition to the magnitude of surface stress, the depth of compressive stress is an equally important metric for fatigue resistance, as deeper stresses help reduce the effective stress around potential anomalies or near-surface stress

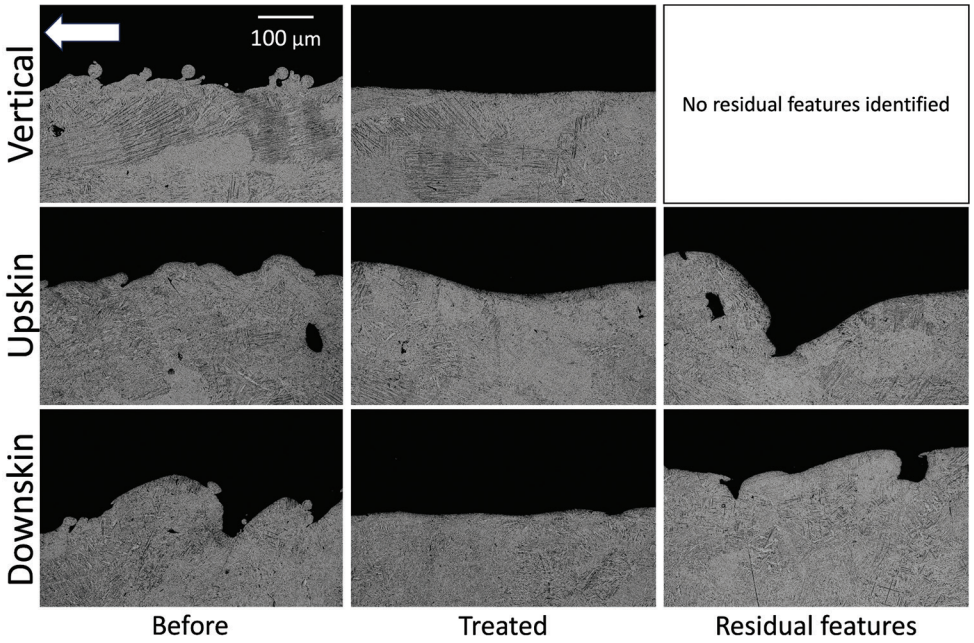

Figure 11. Cross-sectional images of printed samples with vertical, upskin, and downskin surfaces. The build direction is indicated by the arrow. Scale bar: 100 µm

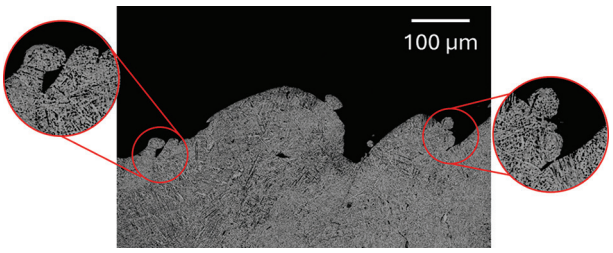

Figure 12. Cross-sectional view of a representative area of a downskin surface in the as-built condition, highlighting potential hidden valleys that are shielded from treatment

concentrations. Subsurface mapping (Figure 10) indicated a plateau in residual stress at a depth of approximately 30 µm. Shot peening, the mainstream surface treatment, can introduce residual stress up to depths of 150 µm or more below the surface.[65,66] Thus, when compared to shot peening, CASF has a lower depth of residual stress penetration within the range of treatment conditions used. However, the depth is compatible with other treatments. Water jet peening has been reported to induce residual stress up to 40 µm below the surface in similar titanium alloys.[43] It is plausible that increasing treatment pressure or intensity could enhance the depth of CASF-induced residual stress, warranting further investigation.

The compressive residual stress resulting from CASF of the upskin surface reached 600 MPa. Assuming that the lower stresses observed on vertical and downskin surfaces result from shielding by partially melted powder particles, it should be feasible to achieve comparable stress levels across all orientations by removing the particles and applying sufficient treatment intensity. Nevertheless, the surface residual stress achieved by CASF exceeds that of tribofinishing (500 MPa) and is similar to shot peening (350–650 MPa),[48,67] while also matching or surpassing recent results for laser cavitation peening (400–450 MPa).[48,49] These findings highlight the considerable potential of CASF as a post-processing technique for L-PBF titanium components, both for enhancing surface quality and introducing compressive residual stresses.[41,48-49,67] While the exact outcomes depend on material properties, similar benefits are anticipated for other metals processed via L-PBF.

Despite the novelty of the findings and new evidence supporting the use of CASF for post-processing L-PBF components, several limitations should be noted. First, the study was limited to Ti6Al4V. While similar results are expected for other sufficiently ductile metals, experimental validation is required to confirm this assumption. Second, the study relied on the use of $\overline{K_t}$ to describe surface stress concentration and quantify the influence of CASF on surface structures relevant to fatigue behavior. The $\overline{K_t}$ approach is considered appropriate for industrial applications due to its simplicity and use of conventional roughness parameters. However, a fracture mechanics approach[68,69] has been proposed to account for the influence of surface notches indicative of L-PBF builds on fatigue, as

well as other treatments based on stress concentration.[70] These alternative approaches were not considered in this study, as they are beyond the scope of the primary objective. Finally, while a major motivation for imposing compressive residual stress is to improve the fatigue life, fatigue testing was not included in this study. As a scoping study, the primary objective was to evaluate the overall potential for CASF to improve the surface integrity of L-PBF components. Future investigations should include fatigue testing post-CASF treatment to validate the anticipated improvements in component performance.

The combined effects of reduced surface roughness, lowered effective stress concentrations, and the introduction of compressive residual stress suggest that CASF could improve the fatigue resistance of metal components regardless of the AM method used. A notable advantage of CASF is its reliance solely on water and abrasives, avoiding the chemical hazards associated with many conventional treatments for Ti6Al4V, which pose risks to both operators and the environment. Nevertheless, the treatment conditions used in this investigation were based on a developing understanding of the process and have not yet been fully optimized. To enable widespread adoption, further work is required to refine CASF parameters for different materials and manufacturing conditions, ensuring consistent and maximized performance.

5. Conclusion

In this study, we evaluated the effect of CASF treatment on the surface texture, stress concentration, and residual stress of Ti6Al4V samples manufactured by L-PBF. In summary, the results showed that:

(i) The CASF process significantly improved surface smoothness for all build orientations, achieving an overall reduction in R_a of up to 50%. The upskin and downskin surfaces exhibited higher initial roughness in the as-built condition, and CASF produced a smaller overall reduction in roughness compared to the vertical orientation. For all surfaces except the upskin, the reduction in surface roughness increased as the treatment feed rate decreased.

(ii) The residual stresses introduced by CASF treatment were compressive for all treatment conditions and were generally independent of feed rate. However, residual stress was highly dependent on the build orientation and the treatment orientation. Although the residual stress reached up to 600 MPa at the surface for the upskin orientation, it decreased with depth to a nearly stress-free state within 30 μm of the treated surface.

(iii) Jet impingement orientation had little effect on the surface roughness achieved by the CASF treatment. However, it significantly affected the residual stress, where oblique impingement angles (<90°) resulted in significantly lower residual stress compared to orthogonal treatment.

(iv) The CASF process reduced the effective surface stress concentration ($\overline{K_t}$) for all treatment conditions and surface orientations, with values in the as-built condition (up to $\overline{K_t} \approx 30$) reduced by as much as a factor of 5. However, the reduction in $\overline{K_t}$ was lowest for the upskin and downskin surfaces, likely due to the limited changes in the profile valley radii.

(v) The effectiveness of CASF treatment—in reducing roughness and introducing residual stress—appeared to depend on the build surface orientation, which is correlated with the presence of unmelted particles. The particles shielded the abrasives and cavitating bubbles, limiting material removal and near-surface deformation.

Acknowledgments

The authors are grateful to Cory Cunningham, Patrick Buffington, and Dr. Reid Schur of the Boeing Company for their encouragement, guidance, and technical discussions.

Funding

The authors gratefully acknowledge that support for this work was provided by the Joint Center for Aerospace Technology Innovation (JCATI) in Washington State. The authors also gratefully acknowledge support for this investigation from The Boeing Company through the Boeing Advanced Research Collaboration and from the Sugino Corporation, Ltd. Part of this work was supported by the Washington Nanofabrication Facility/Molecular Analysis Facility, a National Nanotechnology Coordinated Infrastructure (NNCI) site at the University of Washington with partial support from the National Science Foundation (NNCI-1542101 and NNCI-2025489).

Conflict of interest

Dr. Dan Sanders declares that he is an employee of Sugino Corporation as a chief technical officer, which may be perceived as a conflict.

Author contributions

Conceptualization: Dan Sanders, Mamidala Ramulu, Dwayne Arola

Formal analysis: Rohin Petram, Conall Wisdom, Alex Montelione, Cole Nouwens, Angelina Martinez, Marquiz Silvestre

Investigation: Rohin Petram, Conall Wisdom, Alex Montelione, Cole Nouwens, Angelina Martinez, Marquiz Silvestre

Methodology: Dan Sanders, Mamidala Ramulu, Dwayne Arola
Writing—original draft: Rohin Petram, Conall Wisdom
Writing—review & editing: Alex Montelione, Dan Sanders, Mamidala Ramulu, Dwayne Arola

Ethics approval and consent to participate

Not applicable.

Consent for publication

Not applicable.

Availability of data

Data are available from the corresponding authors upon reasonable request.

References

1. Diegel O, Nordin A, Motte D. A practical guide to design for additive manufacturing. *Springer Series in Advanced Manufacturing*. Berlin: Springer; 2019.

   doi: 10.1007/978-981-13-8281-9_2

2. Galati M, Calignano F, Viccica M, Iuliano L. Additive manufacturing redesigning of metallic parts for high precision machines. *Crystals (Basel)*. 2020;10(3):161.

   doi: 10.3390/cryst10030161

3. Zegard T, Paulino GH. Bridging topology optimization and additive manufacturing. *Struct Multidiscipl Optim*. 2016;53(1):175-192.

   doi: 10.1007/s00158-015-1274-4

4. Allen J. An Investigation into the Comparative Costs of Additive Manufacture vs. Machine from Solid for Aero Engine Parts. In: *Cost Effective Manufacture via Net-Shape Processing*. France: Neuilly-sur-Seine; 2006.

5. Cabanettes F, Joubert A, Chardon G, *et al*. Topography of as built surfaces generated in metal additive manufacturing: A multi scale analysis from form to roughness. *Precis Eng*. 2018;52:249-265.

   doi: 10.1016/j.precisioneng.2018.01.002

6. Elambasseril J, Rogers J, Wallbrink C, Munk D, Leary M, Qian M. Laser powder bed fusion additive manufacturing (LPBF-AM): The influence of design features and LPBF variables on surface topography and effect on fatigue properties. *Crit Rev Solid State Mater Sci*. 2023;48(1):132-168.

   doi: 10.1080/10408436.2022.2041396

7. Gomez-Gallegos A, Mandal P, Gonzalez D, Zuelli N, Blackwell P. Studies on titanium alloys for aerospace application. *Defect Diffus Forum*. 2018;385:419-423.

   doi: 10.4028/www.scientific.net/DDF.385.419

8. Williams JC, Boyer RR. Opportunities and issues in the application of titanium alloys for aerospace components. *Metals (Basel)*. 2020;10(6):705.

   doi: 10.3390/met10060705

9. Boyer RR. An overview on the use of titanium in the aerospace industry. *Mater Sci Eng A*. 1996;213(1):103-114.

   doi: 10.1016/0921-5093(96)10233-1

10. Singh P, Pungotra H, Kalsi NS. On the characteristics of titanium alloys for the aircraft applications. In: *Mater Today: Proceedings*. Vol. 4. Netherlands: Elsevier Ltd.; 2017. p. 8971-8982.

    doi: 10.1016/j.matpr.2017.07.249

11. Bache MR. Processing titanium alloys for optimum fatigue performance. *Int J Fatigue*. 1999;21:S105-S111.

    doi: 10.1016/S0142-1123(99)00061-4

12. Hosseini S. *Fatigue of Ti-6Al-4V*. London: IntechOpen; 2012.

    doi: 10.5772/45753

13. Novovic D, Dewes RC, Aspinwall DK, Voice W, Bowen P. The effect of machined topography and integrity on fatigue life. *Int J Machine Tools Manuf*. 2004;44(2):125-134.

    doi: 10.1016/j.ijmachtools.2003.10.018

14. Javidi A, Rieger U, Eichlseder W. The effect of machining on the surface integrity and fatigue life. *Int J Fatigue*. 2008;30(10):2050-2055.

    doi: 10.1016/j.ijfatigue.2008.01.005

15. Arola D, Williams CL. Estimating the fatigue stress concentration factor of machined surfaces. *Int J Fatigue*. 2002;24(9):923-930.

    doi: 10.1016/S0142-1123(02)00012-9

16. Arola D, Ramulu M. An Examination of the effects from surface texture on the strength of fiber reinforced plastics. *J Compos Mater*. 1999;33(2):102-123.

    doi: 10.1177/002199839903300201

17. Persson BNJ. Surface roughness-induced stress concentration. *Tribol Lett*. 2023;71(2):66.

    doi: 10.1007/s11249-023-01741-4

18. Ye C, Zhang C, Zhao J, Dong Y. Effects of post-processing on the surface finish, porosity, residual stresses, and fatigue performance of additive manufactured metals: A review. *J Mater Eng Perform*. 2021;30(9):6407-6425.

    doi: 10.1007/s11665-021-06021-7

19. Pegues J, Roach M, Scott Williamson R, Shamsaei N. Surface roughness effects on the fatigue strength of additively manufactured Ti-6Al-4V. *Int J Fatigue*. 2018;116:543-552.

    doi: 10.1016/j.ijfatigue.2018.07.013

20. Vayssette B, Saintier N, Brugger C, Elmay M, Pessard E.

Surface roughness of Ti-6Al-4V parts obtained by SLM and EBM: Effect on the high cycle fatigue life. *Procedia Eng*. 2018;213:89-97.

doi: 10.1016/j.proeng.2018.02.010

21. Singh K, Sadeghi F, Correns M, Blass T. A microstructure based approach to model effects of surface roughness on tensile fatigue. *Int J Fatigue*. 2019;129:105229.

doi: 10.1016/j.ijfatigue.2019.105229

22. Snyder JC, Thole KA. Understanding laser powder bed fusion surface roughness. *J Manuf Sci Eng*. 2020;142(7):1-37.

doi: 10.1115/1.4046504

23. Whip B, Sheridan L, Gockel J. The effect of primary processing parameters on surface roughness in laser powder bed additive manufacturing. *Int J Adv Manuf Technol*. 2019;103(9-12):4411-4422.

doi: 10.1007/s00170-019-03716-z

24. Obilanade D, Dordlofva C, Törlind P. Surface roughness considerations in design for additive manufacturing - a literature review. In: *Proceedings of the Design Society*. Vol. 1. Cambridge University Press; 2021. p. 2841-2850.

doi: 10.1017/pds.2021.545

25. Khan HM, Karabulut Y, Kitay O, Kaynak Y, Jawahir IS. Influence of the post-processing operations on surface integrity of metal components produced by laser powder bed fusion additive manufacturing: A review. *Mach Sci Technol*. 2020;25(1):118-176.

doi: 10.1080/10910344.2020.1855649

26. Lu D, Liu Z, Wei X, Chen C, Wang D. Effect of post-processing methods on the surface quality of Ti6Al4V fabricated by laser powder bed fusion. *Front Mater*. 2023;10:1126749.

doi: 10.3389/fmats.2023.1126749

27. Makhetha WMI, Becker TH, Sacks N. Post-processing framework for as-built LPBF Ti-6Al-4V parts towards meeting industry functional requirements. *JOM (1989)*. 2022;74(3):764-776.

doi: 10.1007/s11837-021-05078-y

28. Triantaphyllou A, Giusca CL, Macaulay GD, *et al*. Surface texture measurement for additive manufacturing. *Surf Topogr Metrol Prop*. 2015;3(2):24002.

doi: 10.1088/2051-672X/3/2/024002

29. Covarrubias EE, Eshraghi M. Effect of build angle on surface properties of nickel superalloys processed by selective laser melting. *JOM (1989)*. 2018;70(3):336-342.

doi: 10.1007/s11837-017-2706-y

30. Leach RK, Bourell D, Carmignato S, Donmez A, Senin N, Dewulf W. Geometrical metrology for metal additive manufacturing. *CIRP Ann*. 2019;68(2):677-700.

doi: 10.1016/j.cirp.2019.05.004

31. Rott S, Ladewig A, Friedberger K, Casper J, Full M, Schleifenbaum JH. Surface roughness in laser powder bed fusion - Interdependency of surface orientation and laser incidence. *Add Manuf*. 2020;36:101437.

doi: 10.1016/j.addma.2020.101437

32. Shange M, Yadroitsava I, Pityana S, Yadroitsev I, Bester D. Surface morphology characterisation for parts produced by the high speed selective laser melting. *IOP Conf Ser Mater Sci Eng*. 2019;655(1):12045.

doi: 10.1088/1757-899X/655/1/012045

33. Lizzul L, Bertolini R, Ghiotti A, Bruschi S. Effect of AM-induced anisotropy on the surface integrity of laser powder bed fused Ti6Al4V machined parts. *Proc Manuf*. 2020;47:505-510.

doi: 10.1016/j.promfg.2020.04.149

34. Metelkova J, Vanmunster L, Haitjema H, Van Hooreweder B. Texture of inclined up-facing surfaces in laser powder bed fusion of metals. *Add Manuf*. 2021;42:101970.

doi: 10.1016/j.addma.2021.101970

35. Calignano F. Investigation of the accuracy and roughness in the laser powder bed fusion process. *Virtual Phys Prototyp*. 2018;13(2):97-104.

doi: 10.1080/17452759.2018.1426368

36. Jurg M, Medvedev AE, Yan W, Molotnikov A. Surface improvement of laser powder bed fusion processed Ti6Al4V for fatigue applications. *Add Manuf Lett*. 2022;3:100070.

doi: 10.1016/j.addlet.2022.100070

37. Soe AN, Sombatmai A, Promoppatum P, Srimaneepong V, Trachoo V, Pandee P. Effect of post-processing treatments on surface roughness and mechanical properties of laser powder bed fusion of Ti-6Al-4V Effect of post-processing treatments on surface roughness and mechanical properties of laser powder bed fusion of Ti-6Al-4V. *J Mater Res Technol*. 2024;32:3788-3803.

38. Risposi T, Rusnati L, Patriarca L, Hardaker A, Luczyniec D, Beretta S. Fatigue of Ti6Al4V manufactured by PBF-LB: A comparison of failure mechanisms between net-shape and electro-chemically milled surface conditions. *Eng Failure Anal*. 2025;172:109403.

doi: 10.1016/j.engfailanal.2025.109403

39. Bertolini JC. Hydrofluoric acid: A review of toxicity. *J Emerg Med*. 1992;10(2):163-168.

doi: 10.1016/0736-4679(92)90211-B

40. Kahlin M, Ansell H, Basu D, *et al*. Improved fatigue strength of additively manufactured Ti6Al4V by surface post processing. *Int J Fatigue*. 2020;134:105497.

doi: 10.1016/j.ijfatigue.2020.105497

41. Maleki E, Bagherifard S, Bandini M, Guagliano M. Surface

post-treatments for metal additive manufacturing: Progress, challenges, and opportunities. *Add Manuf* 2021;37:101619.

doi: 10.1016/j.addma.2020.101619

42. Grover HJ. *Factors by Which Shot Peening Influences the Fatigue Strength of Parts. SAE Technical Paper 540138*; 1954.

doi: 10.4271/540138

43. Huang L, Kinnell P, Shipway PH. Removal of heat-formed coating from a titanium alloy using high pressure waterjet: Influence of machining parameters on surface texture and residual stress. *J Mater Process Technol*. 2015;223:129-138.

doi: 10.1016/j.jmatprotec.2015.03.053

44. Arola DD, McCain ML. Abrasive waterjet peening: A new method of surface preparation for metal orthopedic implants. *J Biomed Mater Res*. 2000;53(5):536-546.

doi: 10.1002/1097-4636(200009)53:5<536:AID-JBM13>3.0.CO;2-V

45. Arola D, Alade AE, Weber W. Improving fatigue strength of metals using abrasive waterjet peening. *Mach Sci Technol*. 2006;10(2):197-218.

doi: 10.1080/10910340600710105

46. Yao SL, Wang GY, Yu H, *et al*. Influence of submerged micro-abrasive waterjet peening on surface integrity and fatigue performance of TA19 titanium alloy. *Int J Fatigue*. 2022;164:107076.

doi: 10.1016/j.ijfatigue.2022.107076

47. Soyama H. Cavitation peening: A review. *Metals (Basel)*. 2020;10(2):270.

doi: 10.3390/met10020270

48. Soyama H, Korsunsky AM. A critical comparative review of cavitation peening and other surface peening methods. *J Mater Process Technol*. 2022;305:117586.

doi: 10.1016/j.jmatprotec.2022.117586

49. Soyama H, Kuji C. Improving effects of cavitation peening, using a pulsed laser or a cavitating jet, and shot peening on the fatigue properties of additively manufactured titanium alloy Ti6Al4V. *Surf Coat Technol*. 2022;451:129047.

doi: 10.1016/j.surfcoat.2022.129047

50. Soyama H, Iga Y. Laser cavitation peening: A review. *Appl Sci*. 2023;13(11):6702.

doi: 10.3390/app13116702

51. Sato M, Takakuwa O, Nakai M, Niinomi M, Takeo F, Soyama H. Using cavitation peening to improve the fatigue life of titanium alloy Ti-6Al-4V manufactured by electron beam melting. *Mater Sci Appl*. 2016;7(4):181-191.

doi: 10.4236/msa.2016.74018

52. Petram R, Wisdom C, Montelione A, *et al*. Removing alpha case from laser powder bed fusion components by cavitation abrasive surface finishing. *Materials*. 2025;18(9):1977.

doi: 10.3390/ma18091977

53. ASTM International. *F2924-14: Standard Specification for Additive Manufacturing Titanium-6 Aluminum-4 Vanadium with Powder Bed Fusion*. Vol. 1. United States: ASTM International; 2021.

54. Standard Terminology for Additive Manufacturing Coordinate Systems and Test Methodologies ASTM Standard: ISO/ASTM 52921-13 (Reapproved 2019), ASTM International, United States.

55. International Organization for Standardization, ISO 4288:1998. *Geometrical Product Specifications (GPS) - Surface Texture: Profile Method - Rules and Procedures for the Assessment of Surface Texture, Geometrical Product Specifications (GPS)*. Vol. 1998. United Kingdom: International Organization for Standardization; 1998.

56. Noyan IC, Cohen JB. *Residual Stress: Measurement by Diffraction and Interpretation*. Berlin: Springer-Verlag; 1987.

57. He BB. *Two-Dimensional x-Ray Diffraction*. 2nd ed. United States: John Wiley & Sons, Inc.; 2018. p. 249-325.

58. ASTM E407-07. *Designation: E407- 07 (Reapproved 2015) Standard Practice for Microetching Metals and Alloys*. United States: ASTM International; 2015.

59. Soyama H, Okura Y. The use of various peening methods to improve the fatigue strength of titanium alloy Ti6Al4V manufactured by electron beam melting. *AIMS Mater Sci*. 2018;5(5):1000-1015.

doi: 10.3934/matersci.2018.5.1000

60. Du Plessis A, Beretta S. Killer notches: The effect of as-built surface roughness on fatigue failure in AlSi10Mg produced by laser powder bed fusion. *Add Manuf*. 2020;35:101424.

doi: 10.1016/j.addma.2020.101424

61. Vilardell AM, Krakhmalev P, Fredriksson G, *et al*. Influence of surface topography on fatigue behavior of Ti6Al4V alloy by laser powder bed fusion. In: *Procedia CIRP*. Vol. 74. Elsevier B.V; 2018. p. 49-52.

doi: 10.1016/j.procir.2018.08.028

62. Barricelli L, Patriarca L, du Plessis A, Beretta S. A comparison of fatigue analysis methods for L-PBF net-shape surfaces in Ti6Al4V parts. *Theor Appl Fracture Mech*. 2023;128:104143.

doi: 10.1016/j.tafmec.2023.104143

63. Nicoletto G. Influence of rough as-built surfaces on smooth and notched fatigue behavior of L-PBF AlSi10Mg. *Add Manuf*. 2020;34:101251.

doi: 10.1016/j.addma.2020.101251

64. Simson D, Subbu SK. Effect of process parameters on surface integrity of LPBF Ti6Al4V. *Proceedia CIRP*. 2022;108: 716-721.

doi: 10.1016/j.procir.2022.03.111

65. Wang N, Zhu J, Liu B, Zhang X, Zhang J, Tu S. Influence of ultrasonic surface rolling process and shot peening on fretting fatigue performance of Ti-6Al-4V. *Chin J Mech Eng*. 2021;34(1):1-13.

doi: 10.1186/s10033-021-00611-1

66. Li K, Fu XS, Li RD, *et al*. Fretting fatigue characteristic of Ti–6Al–4V strengthened by wet peening. *Int J Fatigue*. 2016;85:65-69.

doi: 10.1016/j.ijfatigue.2015.12.013

67. Mancisidor AM, García-Blanco MB, Quintana I, *et al*. Effect of post-processing treatment on fatigue performance of Ti6Al4V alloy manufactured by laser powder bed fusion. *J Manuf Mater Process*. 2023;7(4):119.

doi: 10.3390/jmmp7040119

68. Rigon D, Coppola F, Meneghetti G. Fracture mechanics-based analysis of the fatigue limit of Ti6Al4V alloy specimens manufactured by SLM in as-built surface conditions by means of areal measurements. *Eng Fracture Mech*. 2024;295:109720.

doi: 10.1016/j.engfracmech.2023.109720

69. Meneghetti G, Rigon D, Gennari C. An analysis of defects influence on axial fatigue strength of maraging steel specimens produced by additive manufacturing. *Int J Fatigue*. 2019;118:54-64.

doi: 10.1016/j.ijfatigue.2018.08.034

70. Lee S, Rasoolian B, Silva DF, Pegues JW, Shamsaei N. Surface roughness parameter and modeling for fatigue behavior of additive manufactured parts: A non-destructive data-driven approach. *Addit Manuf*. 2021;46:102094.

doi: 10.1016/j.addma.2021.102094